# The formation and characterization of cyclodextrin functionalized polystyrene nanofibers produced by electrospinning

Nanotechnology **20** (2009) 125605 (14pp) doi:10.1088/0957-4484/20/12/125605

# The formation and characterization of cyclodextrin functionalized polystyrene nanofibers produced by electrospinning

**Tamer Uyar[1,4], Rasmus Havelund[1], Jale Hacaloglu[2], Xingfei Zhou[1], Flemming Besenbacher[1,3] and Peter Kingshott[1]**

[1] Interdisciplinary Nanoscience Center (iNANO), Aarhus University, DK-8000, Aarhus C, Denmark
[2] Department of Chemistry, Middle East Technical University, Ankara 06530, Turkey
[3] Department of Physics and Astronomy, Aarhus University, DK-8000, Aarhus C, Denmark

E-mail: tamer@inano.dk and tamer@unam.bilkent.edu.tr

Received 20 November 2008, in final form 19 January 2009
Published 4 March 2009
Online at stacks.iop.org/Nano/20/125605

**Abstract**

Polystyrene (PS) nanofibers containing the inclusion complex forming beta-cyclodextrin ($\beta$-CD) were successfully produced by electrospinning aimed at developing functional fibrous nanowebs. By optimization of the electrospinning parameters, which included varying the relative concentration of PS and $\beta$-CD in the solutions, bead-free fibers were produced. Homogeneous solutions of $\beta$-CD and PS in dimethylformamide (DMF) were used with concentrations of PS varying from 10% to 25% (w/v, with respect to DMF), and $\beta$-CD concentrations of 1% to 50% (w/w, with respect to PS). The presence of $\beta$-CD facilitated the production of bead-free PS fibers even from lower polymer concentrations as a result of the higher conductivity of the PS/CD solutions. The morphology and the production of bead-free PS/CD fibers were highly dependent on the $\beta$-CD contents. Transmission electron microscope (TEM) and atomic force microscope (AFM) images showed that incorporation of $\beta$-CD yielded PS fibers with rougher surfaces. Thermogravimetric analysis (TGA) and direct insertion probe pyrolysis mass spectroscopy (DP-MS) results confirmed the presence of $\beta$-CD in the PS fibers. X-ray diffraction (XRD) spectra of the fibers indicated that the $\beta$-CD molecules are distributed within the PS matrix without any phase separated crystalline aggregates up to 40% (w/w) $\beta$-CD loading. Furthermore, chemical analyses by Fourier transform infrared (FTIR) spectroscopy studies confirm that $\beta$-CD molecules are located within the PS fiber matrix. Finally, preliminary investigations using x-ray photoelectron spectroscopy (XPS) and time-of-flight *static* secondary ion mass spectrometry (ToF-static-SIMS) show the presence of the cyclodextrin molecules in the outer molecular layers of the fiber surfaces. The XPS and ToF-SIMS findings indicate that cyclodextrin functionalized PS webs would have the potential to be used as molecular filters and/or nanofilters for the purposes of filtration/purification/separation owing to surface associated $\beta$-CD molecules which have inclusion complexation capability.

(Some figures in this article are in colour only in the electronic version)

## 1. Introduction

Electrospinning is a very versatile and cost effective process for producing nanofibers from various polymers, polymer blends, sol–gels, composites, ceramics, etc [1, 2]. Nanofibers/nanowebs produced by the electrospinning technique have several remarkable characteristics, such as a very large surface area to volume ratio and pore sizes within the nanoscale range. Additionally, the modification and functionalization of electrospun nanofibers is possible through the electrospinning of a polymer matrix by incor-

[4] Author to whom any correspondence should be addressed. Present address: UNAM-Institute of Materials Science and Nanotechnology, Bilkent University, Ankara, 06800, Turkey.

 

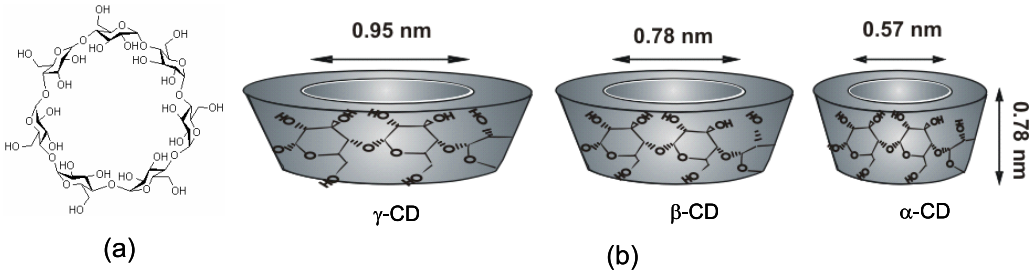


**Figure 1.** (a) Chemical structure of $\beta$-CD, (b) approximate dimensions of $\alpha$-CD, $\beta$-CD, and $\gamma$-CD.

**Table 1.** The characteristics of PS and PS/$\beta$-CD solutions and the resulting electrospun fibers.

| Solutions | % PS[a] (w/v) | % $\beta$-CD[b] (w/w) | Viscosity (cP) | Conductivity ($\mu$S cm$^{-1}$) | Fiber diameter (nm) | Bead size (length/width, $l/w$) ($\mu$m) | Bead aspect ratio | Fiber morphology |
|---|---|---|---|---|---|---|---|---|
| PS10 | 10 | — | 22.9 ± 0.06 | 2.5 | 166 ± 47 | 10.20 ± 1.99/7.61 ± 0.92 | 1.36 ± 0.33 | Nanofibers with many beads |
| PS10/CD1 | 10 | 1 | 21.1 ± 0.06 | 2.6 | 199 ± 49 | 7.71 ± 1.60/4.54 ± 1.08 | 1.76 ± 0.46 | Nanofibers with many beads |
| PS10/CD10 | 10 | 10 | 21.2 ± 0.2 | 3.2 | 251 ± 53 | 8.09 ± 1.52/3.91 ± 1.04 | 2.18 ± 0.62 | Nanofibers with many beads |
| PS10/CD25 | 10 | 25 | 20.7 ± 0.2 | 4.1 | 457 ± 96 | 8.63 ± 1.75/3.31 ± 0.96 | 2.78 ± 0.86 | Nanofibers with few beads |
| PS10/CD40 | 10 | 40 | 20.3 ± 0.2 | 4.9 | 899 ± 176 | 14.04 ± 3.08/3.53 ± 0.72 | 3.97 ± 0.33 | Nanofibers with very few beads |
| PS10/CD50 | 10 | 50 | 21.1 ± 0.3 | 5.3 | 1161 ± 271 | — | — | Bead-free nanofibers and microfibers |
| PS15 | 15 | — | 59.9 ± 0.5 | 1.35 | 381 ± 95 | 10.45 ± 1.56/6.30 ± 0.90 | 1.69 ± 0.34 | Nanofibers with many beads |
| PS15/CD1 | 15 | 1 | 59.6 ± 0.6 | 1.7 | 505 ± 124 | 11.70 ± 2.13/5.08 ± 1.50 | 2.46 ± 0.66 | Nanofibers with many beads |
| PS15/CD10 | 15 | 10 | 57.9 ± 0.7 | 2.7 | 660 ± 157 | 10.99 ± 1.56/4.01 ± 0.87 | 2.84 ± 0.65 | Nanofibers with very few beads |
| PS15/CD25 | 15 | 25 | 60.6 ± 0.2 | 3.8 | 1214 ± 279 | — | — | Bead-free nanofibers and microfibers |
| PS20 | 20 | — | 138.3 ± 0.7 | 1.1 | 827 ± 166 | 12.49 ± 2.46/5.53 ± 1.16 | 2.34 ± 0.65 | Nanofibers with beads |
| PS20/CD1 | 20 | 1 | 140.1 ± 1.1 | 1.4 | 1080 ± 138 | 13.89 ± 1.91/5.80 ± 0.84 | 2.42 ± 0.35 | Nanofibers and microfibers with beads |
| PS20/CD5 | 20 | 5 | 141.7 ± 0.8 | 2.1 | 1399 ± 189 | 15.22 ± 3.35/5.64 ± 1.27 | 2.74 ± 0.49 | Microfibers with very few beads |
| PS20/CD10 | 20 | 10 | 146.9 ± 0.7 | 2.4 | 1610 ± 186 | — | — | Bead-free microfibers |
| PS25 | 25 | — | 240.4 ± 1.5 | 1.1 | 1959 ± 162 | — | — | Bead-free microfibers |

[a] With respect to solvent (DMF).
[b] With respect to polymer (PS).

porating functional additives [3, 4]. It has been reported that the unique properties and multifunctionality of such nanofibers/nanowebs make them favorable candidates to be used in various applications areas including biotechnology, textiles, membranes/filters, composites, sensors, fuel and solar cells, and electronics [1, 2, 5–9].

Cyclodextrins (CDs) are cyclic oligosaccharides consisting of $\alpha(1,4)$-linked glucopyranose units having a toroid-shaped molecular structure (figure 1). The most common natural CDs either have 6, 7, or 8 glucopyranose units in the cycle and are named $\alpha$-CD, $\beta$-CD, and $\gamma$-CD, respectively. The CD cavity acts as a host for various small molecules [10–12] as well as macromolecules [13–15] to form noncovalent host–guest inclusion complexes. The functionalization of nanofibers with cyclodextrins would be extremely appealing since such nanowebs containing CDs will have unique characteristics that can potentially improve and broaden the application areas of cyclodextrins and nanofibers. For instance, fibrous mats consisting of nanofibers have the potential to be used for the filtration of tiny particles as well as for the purification of industrial waste since they have large surface area along with a nanoporous structure [7, 16].

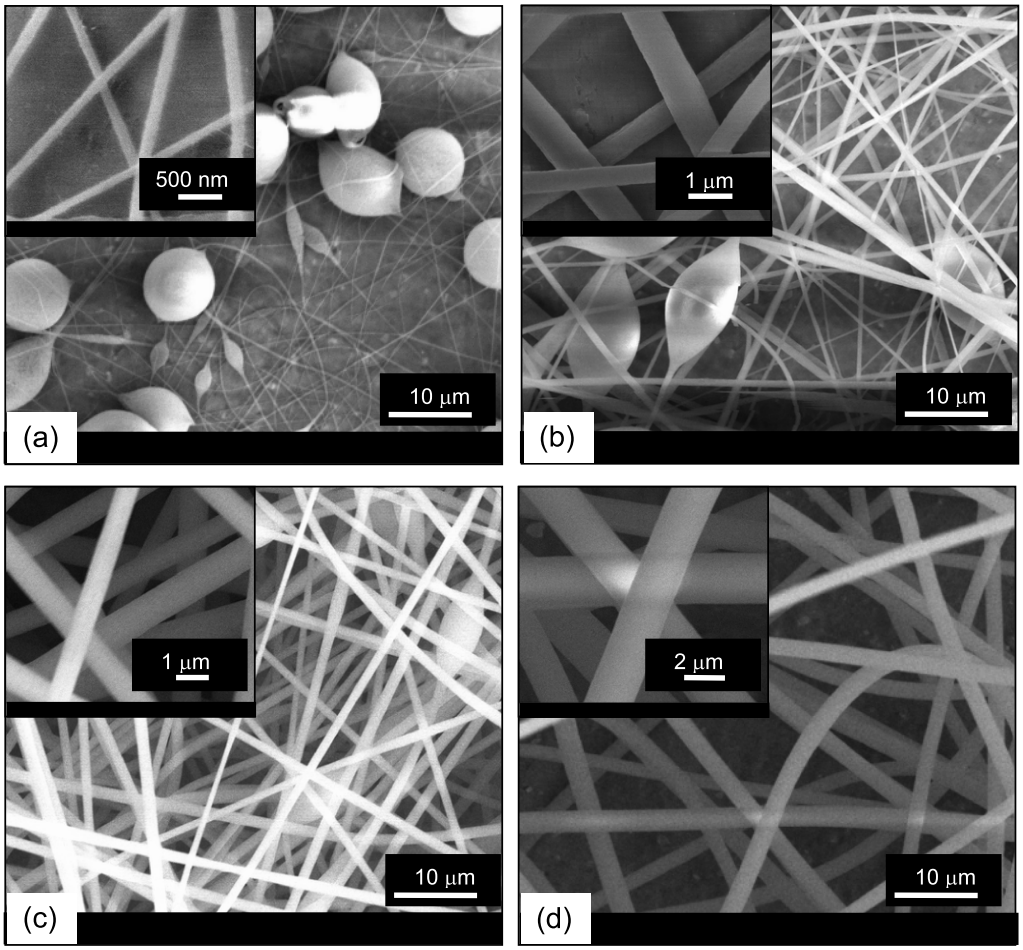


**Figure 2.** SEM images of electrospun polystyrene (PS) fibers from DMF solution at a concentration of (a) 10%, (b) 15%, (c) 20%, and (d) 25% (w/v). The insets show higher magnification images.

Cyclodextrins have the ability to entrap molecules and they can remove polluting substances (e.g. organic molecules, heavy metals, radioactive wastes, etc) from the environment by forming inclusion complexation [17–19]. Hence, CD functionalized electrospun nanofibers can potentially be used as molecular filters and/or nanofilters for filtration/purification/separation purposes [20–22].

In this study, beta-cyclodextrin ($\beta$-CD) functionalized polystyrene (PS) nanofibers (PS/CD) were successfully produced by an electrospinning technique with the goal of developing functional fibrous nanowebs. The weight load of $\beta$-CD in the PS matrix was varied from 1% up to 50% (w/w). We found that the presence of CD increases the conductivity of the polymer solutions and this assists the electrospinning process of PS from lower polymer concentration, yielding bead-free PS/CD fibers. This study mainly deals with the optimization of electrospinning conditions in order to produce uniform PS/CD nanofibers with different $\beta$-CD content. In addition, characterizations of these PS/CD nanofibers/nanowebs were carried out extensively by using a scanning electron microscope (SEM), transmission electron microscope (TEM), atomic force microscope (AFM), thermogravimetric analysis (TGA), direct insertion probe pyrolysis mass spectroscopy (DP-MS), x-ray diffraction (XRD), and Fourier transform infrared spectroscopy (FTIR). Surface characterization by x-ray photoelectron spectroscopy (XPS) and time-of-flight *static* secondary ion mass spectrometry (ToF-static-SIMS) allowed for detection of $\beta$-CD molecules in the outer molecular layers of the fiber surface where they are intended to function. Furthermore, we found that these nanowebs were able to capture organic molecules (e.g. phenolphthalein) from the solution, but the detailed study of the molecular filtration capability of these PS/CD nanowebs is discussed elsewhere [22].

## 2. Experimental details

### *2.1. Materials*

Amorphous polystyrene (PS) ($M_w \sim 280\,000$) and $N,N$-dimethylformamide (DMF) (99%) were purchased from Aldrich, and beta-cyclodextrin ($\beta$-CD) was a gift from Wacker Chemie AG, Germany. The materials were used without any purification.

### *2.2. Electrospinning*

Homogeneous solutions of PS/CD were prepared by dissolving PS and $\beta$-CD in DMF. The PS concentration was varied from 10% to 25% (w/v, with respect to solvent) and the weight%

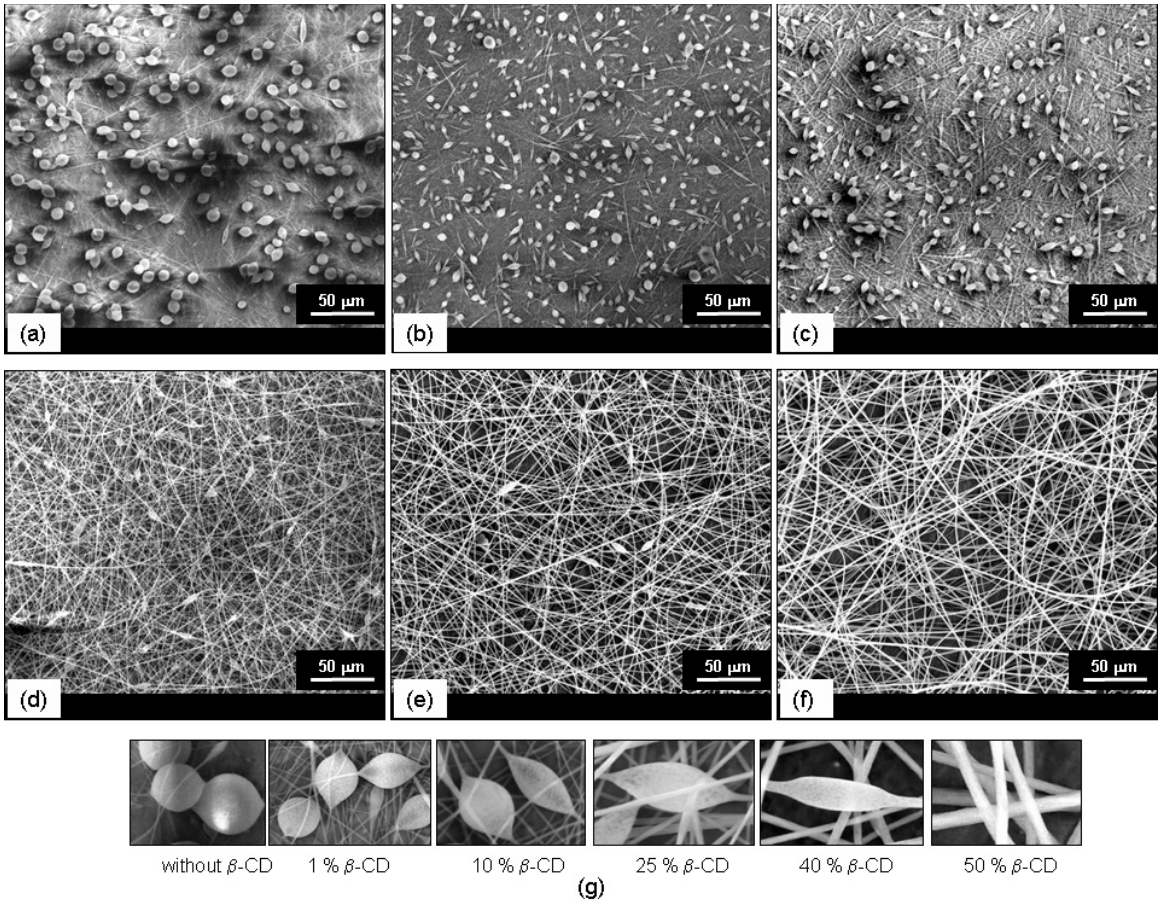


**Figure 3.** SEM images of electrospun fibers of (a) PS10, (b) PS10/CD1, (c) PS10/CD10, (d) PS10/CD25, (e) PS10/CD40, and (f) PS10/CD50. (g) The change of bead morphology in PS/CD fibers with the addition of $\beta$-CD (note: the images are not at the same magnification).

of $\beta$-CD was varied from 1% to 50% (w/w, with respect to PS) (table 1). The polymer solutions were placed in a 1 ml syringe fitted with a metallic needle with 0.4 mm inner diameter. The syringe was fixed horizontally on a syringe pump (Model: KDS 101, KD Scientific) and the electrode of the high voltage power supply (Spellman High Voltage Electronics Corporation, MP Series) was clamped to the metal needle tip. The feed rates of the polymer solutions were varied from 0.5 to 2 ml $h^{-1}$, the applied voltage was varied from 10 to 25 kV, and the tip-to-collector distance was varied from 5 to 15 cm. The most uniform, reproducible and finest fibers were obtained for a feed rate = 1 ml $h^{-1}$, applied voltage = 15 kV, and tip-to-collector distance = 10 cm. Therefore, these parameters were employed for the electrospinning of the polymer solutions studied. A grounded stationary rectangular metal collector (15 cm × 20 cm) covered by a piece of aluminum foil was used as the target for the fiber deposition. The complete electrospinning apparatus was enclosed in a glass box and the electrospinning was carried out at room temperature in a horizontal position.

### *2.3. Measurements and characterizations*

The viscosity of the solutions was measured at 24 °C using a Brookfield DV-III Ultra rheometer, which is equipped with a cone/plate accessory of spindle type CPE-41. The viscosity measurements were repeated three times to check the reproducibility and the consistency of the viscosity reading. The conductivity of the solutions was measured with Multiparameter meter InoLab® Multi 720 (WTW) at room temperature.

The morphologies of the electrospun polystyrene (PS) and cyclodextrin (CD) functionalized PS fibers (PS/CD) were investigated with a high resolution scanning electron microscope (SEM) (FEI, Nova 600 NanoSEM), an atomic force microscope (AFM) (JPK NanoWizard II), and a transmission electron microscope (TEM) (Philips CM20). The average fiber diameter (AFD) and the aspect ratio of the beads were determined from the SEM images, and around 50 fibers and 25 beads were analyzed. The AFM imaging of fibers collected on a microscope slide was performed in intermittent contact mode in air with a scan rate of 0.4–1.2 Hz, and a cantilever NSG 10 (ND-MDT) with resonant frequency = 190–325 kHz tip having a spring constant of 5.5–22.5 N $m^{-1}$ was used. The cross-sections of the fibers were analyzed from AFM images by using JPK software. TEM imaging of the fibers positioned on a copper grid was carried out at 200 kV.

Fourier transform infrared (FTIR) spectroscopy studies were performed with a Perkin Elmer FTIR spectrometer (Paragon 1000). The samples were blended with potassium bromide (KBr) and pellets were formed under high pressure. The spectra were recorded with a resolution of 2 $cm^{-1}$ and

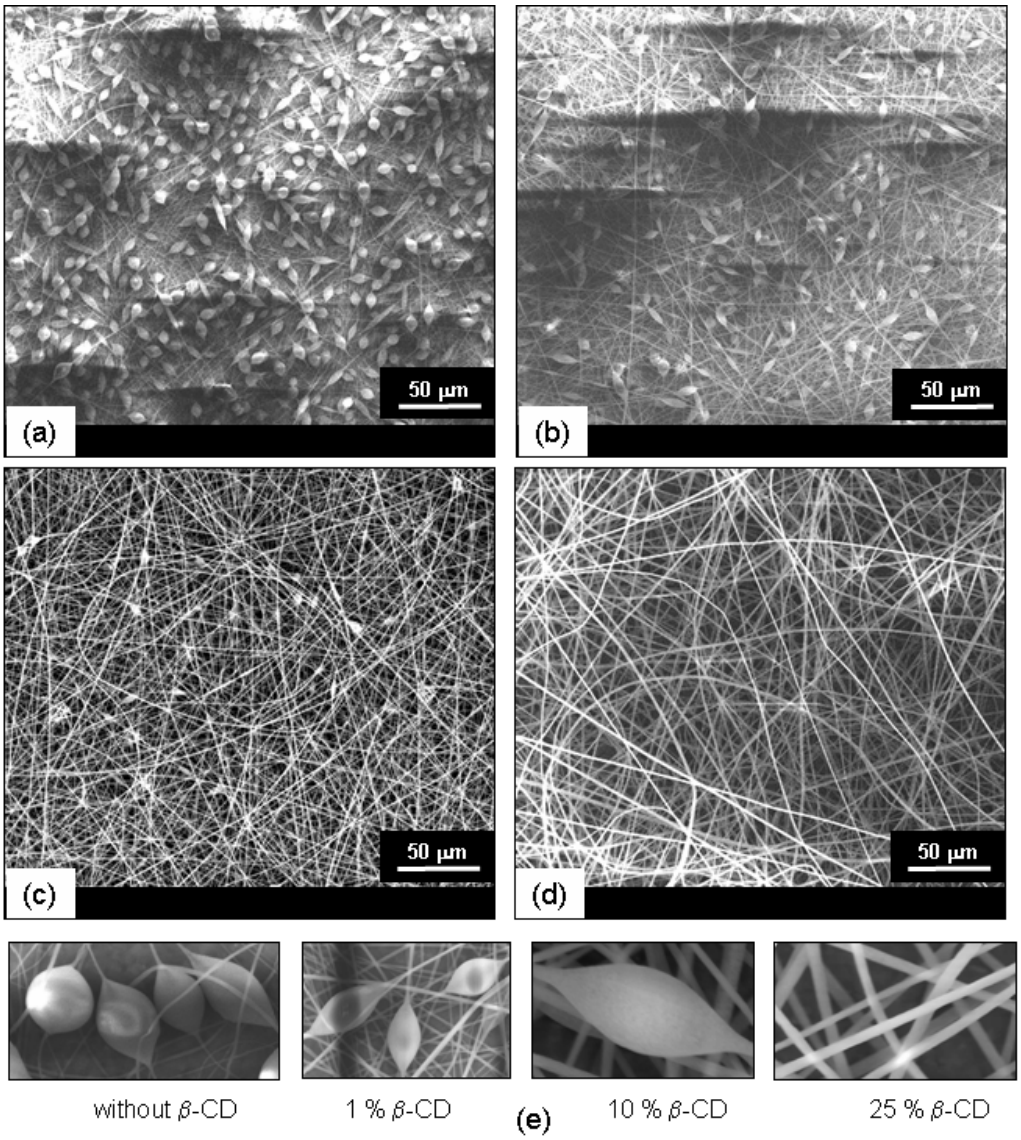


**Figure 4.** SEM images of electrospun fibers of (a) PS15, (b) PS15/CD1, (c) PS15/CD10, and (d) PS15/CD25. (e) The change of bead morphology in PS/CD fibers with the addition of $\beta$-CD (note: the images are not at the same magnification).

averaged over 16 scans. The x-ray diffraction (XRD) data for PS and PS/CD nanowebs were recorded using a Stoe Stadi P diffractometer with Cu K$\alpha$ radiation in a $2\theta$ range 5°–30°. Thermal analyses of the fibers were carried out by using thermal gravimetric analysis (TGA) and direct insertion probe pyrolysis mass spectrometry (DP-MS). TGA was performed using a Netsch STA 409 thermal analyzer. About 10 mg of fiber samples was heated from room temperature to 500 °C at 10 °C min$^{-1}$. The DP-MS system consists of Waters Quattro Micro GC tandem MS with an EI ion source and a mass range of 10–1500 Da coupled with a direct insertion probe ($T_{max} = 650$ °C). 0.01 mg of each fiber sample was pyrolyzed in flared quartz sample vials. The temperature was increased at a rate of 10 °C min$^{-1}$ and the scan rate was 1 scans s$^{-1}$, with simultaneous mass spectrometric analysis of the pyrolytic fragments.

X-ray photoelectron spectroscopy (XPS) was performed using a Kratos Axis Ultra$^{DLD}$ instrument equipped with a monochromated Al K$\alpha$ x-ray source ($h\nu = 1486.6$ electron volts (eV)) operating at 10 kV and 15 mA (150 W). The nanofiber samples that were analyzed were cut from Al foil containing a thick layer of fibers. A hybrid lens mode was employed during analysis (electrostatic and magnetic), with an analysis area of approximately 300 $\mu$m × 700 $\mu$m. For each sample, a take-off angle (TOA) of 0° (with respect to the sample surface) was used, allowing a maximum probe depth (10 nm). Wide energy survey scans (WESSs) were obtained over the 0–1400 eV binding energy (BE) range at a pass energy of 160 eV, and used to determine the surface elemental composition. High resolution spectra were recorded for C 1s and O 1s at a detector pass energy of 20 eV. The Kratos charge neutralizer system was used on all samples with a filament current of between 1.8 and 2.1 A and a charge balance of 3.6 V.

ToF-SIMS analysis was performed using an ION-TOF TOF.SIMS 5 instrument equipped with a Bi primary ion cluster source operating at 25 kV. In most cases $Bi_3^+$ primary ions

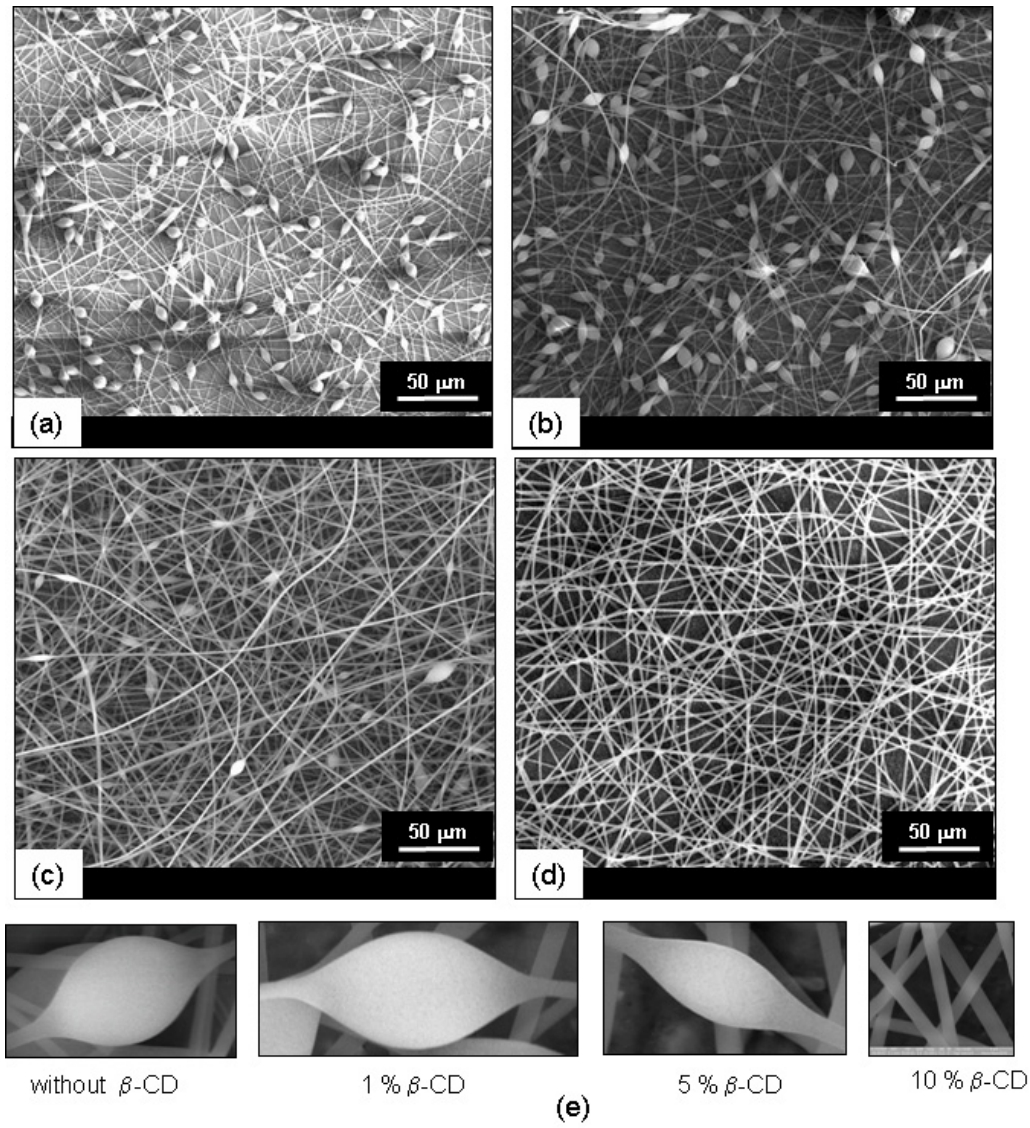


**Figure 5.** SEM images of electrospun fibers of (a) PS20, (b) PS20/CD1, (c) PS20/CD5, and (d) PS20/CD10. (e) The change of bead morphology in PS/CD fibers with the addition of $\beta$-CD (note: the images are not at the same magnification).

were used with a target current of 0.3 pA. High resolution mass spectra ($M/\Delta M > 4000$ at $m/z = 27$) were acquired using the high current bunched mode. High mass resolution spectra were obtained by the use of bunched primary ions. The analysis area was $500 \times 500$ $\mu$m$^2$. Both positive and negative ion secondary ion spectra were acquired. Mass calibration of the positive ion spectra was based on $CH_3^+$, $C_2H_3^+$, $C_2H_5^+$, and $C_3H_5^+$ ions, and the negative ions used for calibration were $C^-$, $CH^-$, $C_2H_2^-$, and $C_3H_3^-$. In all cases an electron flood gun was used for charge compensation and the primary ion dose was kept below $10^{12}$ ions cm$^{-2}$ to stay within the *static* SIMS regime.

## 3. Results and discussion

### *3.1. Electrospinning of polystyrene (PS) fibers*

Initially the electrospinning of polystyrene (PS) fibers with different polymer concentrations was performed in order to find a protocol by means of which we could produce bead-free PS fibers. The concentration of the PS solutions was varied from 10% up to 25% (w/v) in DMF. Table 1 summarizes the solution properties (viscosity and conductivity) of PS and PS/CD and the morphological results for the electrospun fibers. It was found that the viscosity increased as the concentration of polymer solution increased from 10% through 25% (w/v) due to the higher number of polymer chain entanglements. The conductivity of the PS solution is lowered as the weight% of the polymer is increased since PS is a non-conducting polymer. Figure 2 shows the scanning electron microscopy (SEM) images of PS fibers electrospun from 10%, 15%, 20%, and 25% (w/v) PS solution in DMF. It was observed that beaded nanofibers were obtained at the low polymer concentrations, yet the number of beads was reduced significantly and the aspect ratio of beads was higher as the polymer concentration increased from 10% through 20% (w/v). The PS concentration at 25% (w/v) yielded bead-free fibers, which signified that

a high concentration/viscosity is required to obtain bead-free uniform PS fibers. These findings are consistent with previous findings in the literature, where bead-free PS fibers were obtained only in the high concentration/viscosity range [23]. Additionally, the diameter of electrospun PS fibers increased from nanometer to micron range as the concentration of the polymer increased in the solution. This behavior is typically observed in electrospinning processes of concentrated polymer solutions and the increase in fiber diameter is due to the greater resistance of the solution to be stretched since more chain entanglements are present at higher polymer concentration.

### *3.2. Electrospinning of cyclodextrin functionalized polystyrene fibers (PS/CD)*

Cyclodextrin functionalized polystyrene fibers (PS/CD) were produced by electrospinning a homogeneous solution of PS and $\beta$-CD dissolved in DMF. The PS concentration was varied from 10% to 20% (w/v) and the content of $\beta$-CD was varied from 1% to 50% (w/w, with respect to PS) depending on the PS concentration in the solutions (table 1).

Interestingly, it was found that the PS/CD solutions yielded bead-free fibers even when the PS concentrations were well below 25% (w/v). Figure 3 shows SEM images of electrospun PS/CD nanofibers obtained from 10% (w/v) PS with the addition of 1%, 10%, 25%, 40%, and 50% (w/w, with respect to PS) $\beta$-CD. As mentioned above, the 10% (w/v) PS solution yielded vastly beaded nanofibers due to the low viscosity of the polymer solution (figure 3(a)). However, we observed that the addition of $\beta$-CD to the PS solution had a significant effect on the morphology of the resulting electrospun fibers. The addition of $\beta$-CD (1% through 40% (w/w)) reduced the number of beads significantly (figures 3(b)–(e)), and the addition of 50% (w/w) $\beta$-CD yielded uniform bead-free nanofibers (figure 3(f)) from 10% (w/v) PS solution. Additionally, it was observed that beads were more elongated, having higher aspect ratio, as the weight% of $\beta$-CD increased in the polymer solution (figure 3(g) and table 1).

For PS/CD solutions having 15% (w/v) PS, a similar behavior was observed with the addition of $\beta$-CD; that is, the number of beads was reduced significantly (figure 4) and beads with higher aspect ratio were obtained as the concentration of $\beta$-CD increased from 1% through 10% (w/w) (figures 4(b) and (c)). The bead formation was totally eliminated and bead-free fibers were obtained when 25% (w/w) $\beta$-CD was added in the polymer solution (figure 4(d)).

In the case of 20% (w/v) PS, the addition of 1% and 5% (w/w) $\beta$-CD yielded fibers having fewer beads with higher aspect ratio when compared to PS solution without $\beta$-CD (figures 5(a)–(c)). Uniform bead-free PS/CD fibers were produced with the incorporation of 10% (w/w) $\beta$-CD in 20% (w/v) PS solution (figure 5(d)). These findings reveal that the addition of $\beta$-CD has quite a positive effect on the electrospinning of bead-free PS fibers from low polymer concentrations.

The viscosities of the PS and PS/CD solutions containing different weight% of $\beta$-CD were almost the same, indicating

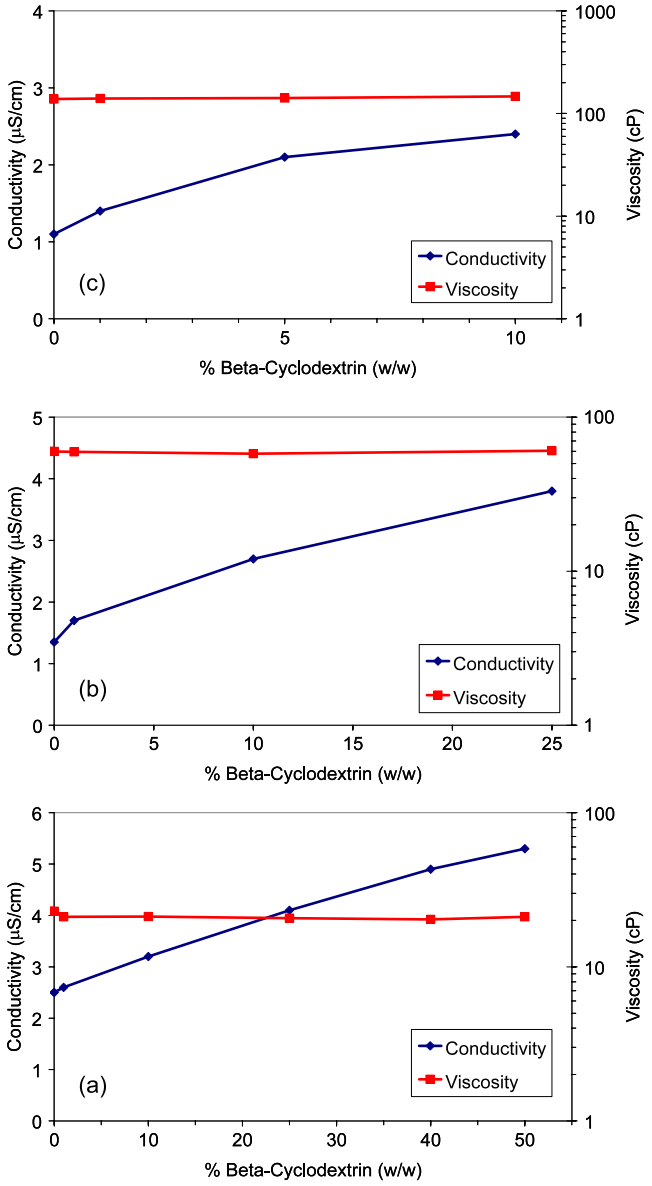


**Figure 6.** Viscosity and conductivity of PS/CD solutions containing different amounts of $\beta$-CD in (a) 10% PS, (b) 15% PS and (c) 20 % PS.

that the addition of CD has no effect on the viscosity of the polymer solution (figure 6 and table 1). This finding shows that the viscosity cannot be the main reason for the yield of different fiber morphologies when $\beta$-CD is added to the PS solutions. It is also worth saying that the possibility of complexation between PS and CD was ruled out since the PS/CD solutions were clear; no turbidity/precipitation was observed, and the viscosity of the PS/CD solutions was steady. In the case of polymer/cyclodextrin inclusion complexation, the solution became turbid due to the aggregation of threaded CD molecules on the polymer chains [13, 14]. Additionally, the viscosity of the polymer solution should increase significantly due to the interactions between polymer chains and cyclodextrin molecules threaded on different polymer chains [24]. However, here the clear appearance of PS/CD solutions and the viscosity data show no indication of

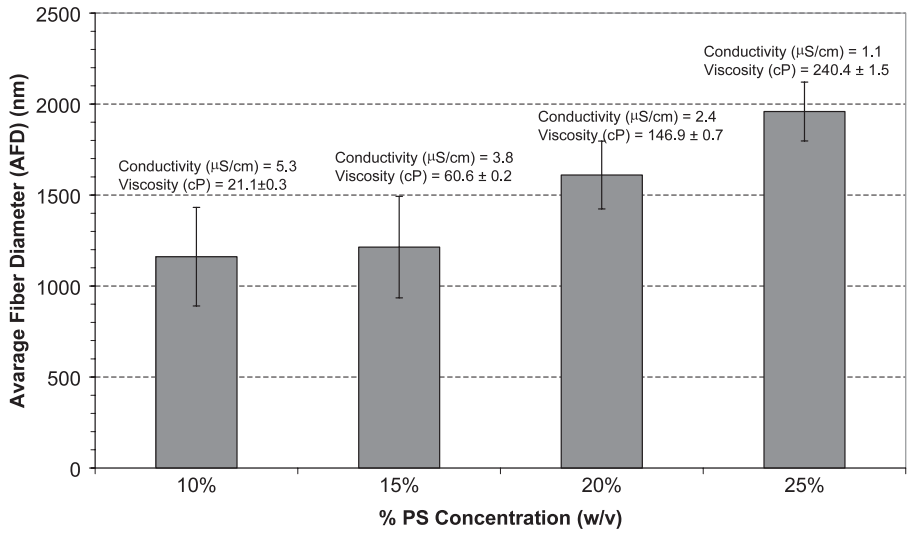


**Figure 7.** Average fiber diameter (AFD) of PS and PS/CD fibers obtained from the electrospinning of different PS concentrations containing different amounts of $\beta$-CD which only yielded bead-free fibers. From left to right, the electrospun fibers are (1) PS10/CD50, (2) PS15/CD25, (3) PS20/CD10, and (4) PS25.

inclusion complexation between $\beta$-CD and PS. This finding correlates with our previous reports in which PS could not form inclusion complexes with CDs, since the cavity of all three CDs ($\alpha$-CD, $\beta$-CD, and $\gamma$-CD) is too narrow to encapsulate amorphous PS chains [25, 26]. So, the $\beta$-CD is present in the PS fiber matrix in a uncomplexed state, and it is important to mention that uncomplexed CD molecules in the polymer matrix are desired since the CD cavity would still be empty and available to perform its function, that is, capture molecules from the surroundings, etc. This is indeed one of the reasons why PS was chosen as the polymer matrix for this study since the polymer matrix is expected not to interfere in the complexation of CD with the target molecules to be captured.

On the other hand, we have found that the conductivity of PS/CD solutions is increased compared to that for pure PS solutions, which implies that the addition of $\beta$-CD causes an increase in the solution conductivity. We also found that the increase in the conductivity was higher as the load of $\beta$-CD was increased (figure 6). A possible reason for the conductivity increase may be the presence of salt impurity in the CD, and indeed sodium ion was detected in the ToF-SIMS analyses. The solution conductivity is one of the main controlling parameters in the electrospinning process, since the polymer solution is being stretched as a result of the repulsion of the charges present at the surface. The increase in conductivity of the solution results in the production of bead-free fibers from lower polymer concentrations since the polymer solution is subjected to higher stretching under the high electrical field [27]. Recently, we have reported that a slight increase in the solution conductivity resulted in significant morphological variations for electrospun PS fibers, yielding bead-free fibers from low polymer concentrations [28]. Here, we observed a similar behavior, where bead-free PS/CD fibers produced from lower polymer concentrations contributed to the high solution conductivity. As expected, the PS/CD systems also yielded thinner fibers due to the characteristics of low viscosity and high conductivity of the solutions. In figure 7 we show the average fiber diameter (AFD) of the PS and PS/CD fibers electrospun from different polymer solutions which only resulted in uniform and bead-free fibers. It is evident that the polymer solutions which have the highest conductivity and lowest viscosity yielded the thinnest fibers; correspondingly, the higher solution conductivity facilitates the production of bead-free fibers from the lower polymer concentrations.

### *3.3. Characterization of cyclodextrin functionalized polystyrene fibers*

The morphological findings of the cyclodextrin functionalized polystyrene fibers (PS/CD) using the SEM were discussed above. In addition, the detailed surface morphology and the surface roughness of the PS and PS/CD fibers were examined with a transmission electron microscope (TEM) and an atomic force microscope (AFM). The TEM images depicted in figure 8 clearly show the presence of some nanopores and ripples on the surface of the PS/CD fibers, and the surface of the PS/CD fibers is rougher when compared to PS fibers. In this case we have analyzed fibers of diameter around 0.5 $\mu$m, although we expect similar findings for larger fibers, which is supported by AFM studies. The AFM images and cross-section profiles of the PS and PS/CD fibers confirm that the incorporation of CD in PS fibers yielded fibers with rougher surfaces (figure 9). The higher the content of CD in the electrospun PS/CD fiber, the rougher is the fiber surface. When volatile solvents are used in the electrospinning of PS fibers, nanosized and microsized pores are obtained on the fiber surface due to the faster evaporation of the lower boiling point solvent [29, 30]. Here we used DMF, which is a high boiling point solvent, for producing uniform PS fibers with smooth surfaces. However, the presence of water in CD may yield rougher surfaces for PS/CD fibers due to rapid evaporation during the electrospinning process. In fact, a rough fiber surface is desired for the PS/CD nanowebs which leads to

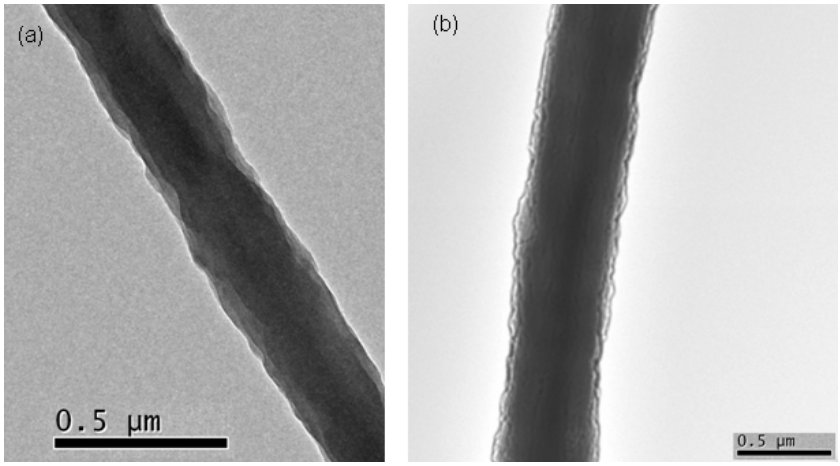


**Figure 8.** TEM images of electrospun fibers: (a) PS10, (b) PS10/CD25.

higher surface area and which can ultimately result in better filtration efficiency.

Thermogravimetric analysis (TGA) is a very useful technique to measure the amount of additives present in the polymer composites if the degradation temperatures of the individual components are distinct from each other. In order to measure the weight percentage of $\beta$-CD in the resulting electrospun PS/CD fibers, TGA experiments were performed. The TGA thermogram of the PS10/CD25 web is given as an example in figure 10. Two distinct weight losses are observed, at around 325–350 °C and 400–440 °C, elucidating the degradation temperature of $\beta$-CD and PS, respectively. It was calculated that the content of $\beta$-CD was about ∼18 wt% in the PS10/CD25 fibers. Initially, 25% (w/w) $\beta$-CD hydrate was mixed with PS, and note that as-received $\beta$-CD hydrate contains about 11–12 moles of water, so the initial amount of $\beta$-CD should be ∼20% (w/w). This calculation matches with the observation from TGA data indicating that the PS/CD solution is homogeneous and that the majority the CD molecules get incorporated into the PS fibers during the process of electrospinning. It is also worth mentioning that typical TGA data for pure cyclodextrins have an initial weight loss (about ∼10%) below 100 °C due to loss of water present in CD [31]. Here, we did not observe any weight loss up to 275 °C, confirming that there is no water present in PS/CD fibers and that the cavities of the CD molecules are free of water.

The thermal behavior of PS and PS/CD fibers was also investigated by direct insertion probe pyrolysis mass spectroscopy (DP-MS). For a multicomponent system, DP-MS allows the separation of components as a function of their volatilities and/or thermal stabilities. In general, DP-MS facilitates analyses of thermal characteristics such as volatility, thermal stability, degradation products, and degradation mechanism of materials, which in turn can be used for investigation of the chemical structures [32, 33]. In pyrolysis MS analysis, not only the detection of a peak, but also the variation of its intensity as a function of temperature, i.e., evolution profile, is important. The trends in the evolution profiles can be used to determine the source of the product, or the mechanism of thermal degradation.

From the DP-MS analyses we observed that the thermal degradation of PS takes place by a free-radical chain reaction, depolymerization, yielding mainly the styrene monomer ($m/z = 104$ Da). The total ion current (TIC) curves (variation of total ion yield as a function of temperature) recorded during the pyrolysis of PS and PS/CD fibers are shown in figure 11. The pyrolysis mass spectra recorded at the maximum of the peaks of TIC (at 440 °C for PS fiber and at 350 and 440 °C for PS/CD fiber) are also presented in the figure. It is clear that two distinct decomposition regimes are present in PS/CD fibers: the degradation of CD in the low temperature region (∼350 °C) and the degradation of PS in the higher temperature region (∼440 °C). $\beta$-CD decomposes by the cleavage of weak C–O bonds, generating intense peaks due to fragments $C_2H_4O_2$ and $C_3H_5O_2$ at $m/z$ values of 60 and 73 Da, respectively. PS degradation takes place by depolymerization of polymer chains, yielding mainly the styrene monomers and oligomers.

In PS/CD fibers, it was observed that the thermal stability of PS was not affected by the presence of CD. However, the relative intensities of monomer (at $m/z = 104$ Da), dimer (at $m/z = 208$ Da), and trimer (at $m/z = 312$ Da) peaks enhanced noticeably in the presence of CD. This indicates that thermal degradation mechanism of PS was somehow affected by the presence of CD. Thermal degradation of PS is a huge environmental issue since carcinogenic degradation products such as benzene are produced during its degradation. In the case of CD functionalized PS fibers used in industrial applications (nanofilters, etc), it is vital to know whether the thermal stability, degradation mechanism, and degradation products are affected by the presence of CD. Currently, we are doing detailed pyrolysis studies on the thermal degradation of CD functionalized PS fibers to investigate the effect of CD on the degradation mechanism and decomposition products of PS fibers. It is also worth mentioning that we did not detect any solvent peaks in the mass spectra during the pyrolysis of PS and PS/CD fibers. DMF is a high boiling point solvent (∼153 °C), and using DMF as a solvent in electrospinning was questioned over using low boiling point solvents such as chloroform [34] since the retention of residual DMF in the electrospun fibers would create toxicity problems. However, our pyrolysis MS

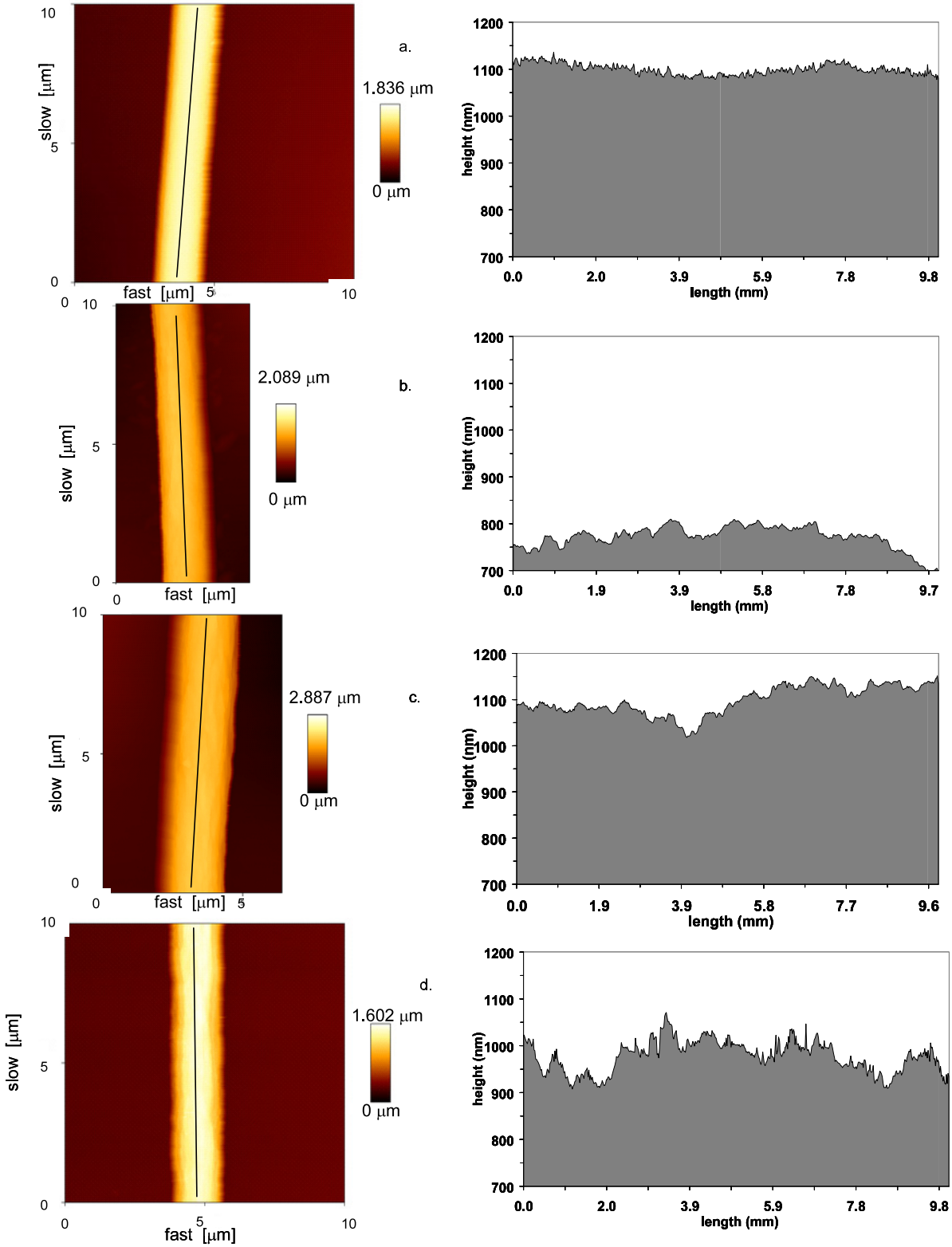


**Figure 9.** AFM images and the cross-section profiles of electrospun fibers: (a) PS25, (b) PS20/CD10, (c) PS15/CD25, and (d) PS10/CD50.

data indicate that the PS and PS/CD fibers are free of solvent molecules.

X-ray diffraction (XRD) is a useful characterization technique for investigating the crystalline structure of CDs. CDs are crystalline and have crystal structures referred to as 'cage' or 'channel' types [35, 36]. The commercially as-received CDs have cage-type packing with an arrangement in which the cavity of each molecule is blocked by neighboring molecules. For the channel-type packing, the CD molecules are aligned and stacked on top of each other, forming

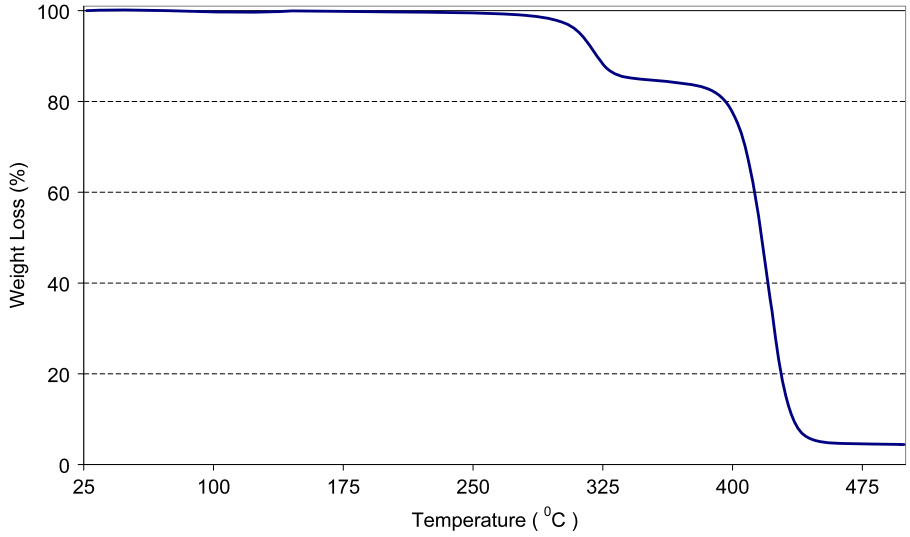


**Figure 10.** TGA thermogram of PS10/CD25 fibers.

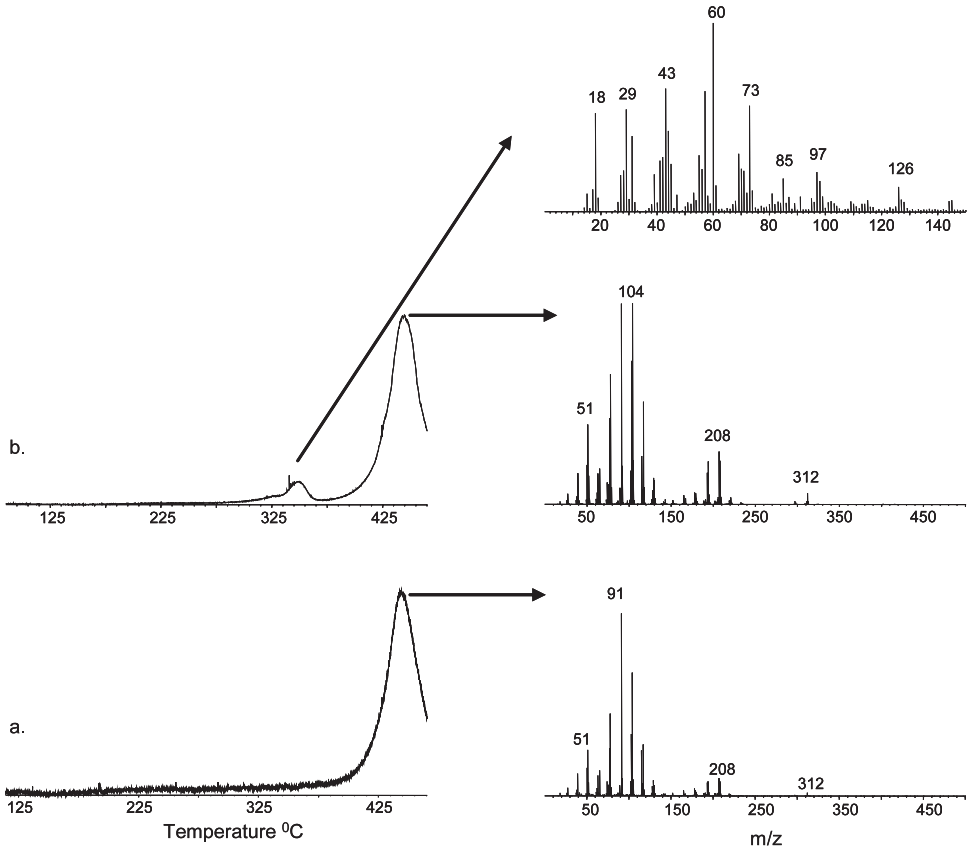


**Figure 11.** The total ion current (TIC) curves and pyrolysis mass spectra recorded at the maximum of the peaks of TIC of (a) PS25 fibers and (b) PS15/CD25 fibers.

long cylindrical channels. CD molecules adopt channel-type packing when the inclusion complexation is formed with lengthy molecules such as polymers [13, 14].

The XRD studies were performed for the PS/CD nanowebs to investigate if any CD crystalline aggregates were present in the fiber matrix. Figure 12 shows the 2D x-ray diffraction (XRD) spectra of PS and PS/CD webs; the XRD pattern of pure $\beta$-CD is also included for comparison. PS is an amorphous polymer with a broad halo diffraction pattern. The XRD diffraction patterns of the PS/CD webs are very similar to that for the PS web, which also depicts a broad halo pattern without any strong diffraction peaks. No distinct peaks for the channel-type $\beta$-CD crystals [13] were observed, indicating that CD and PS did not form inclusion complexes. This finding

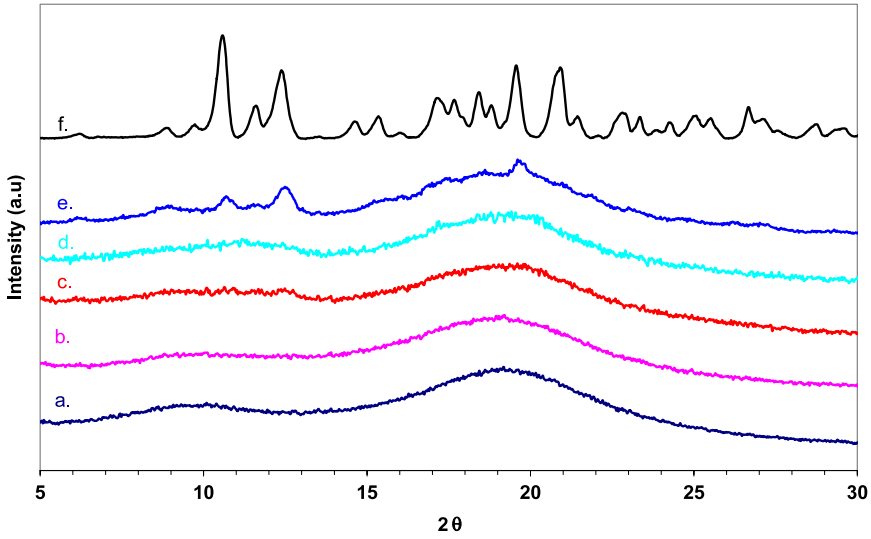


**Figure 12.** 2D XRD patterns of webs of (a) PS25, (b) PS20/CD10, (c) PS15/CD25, (d) PS10/CD40, (e) PS10/CD50, and (f) pure $\beta$-CD.

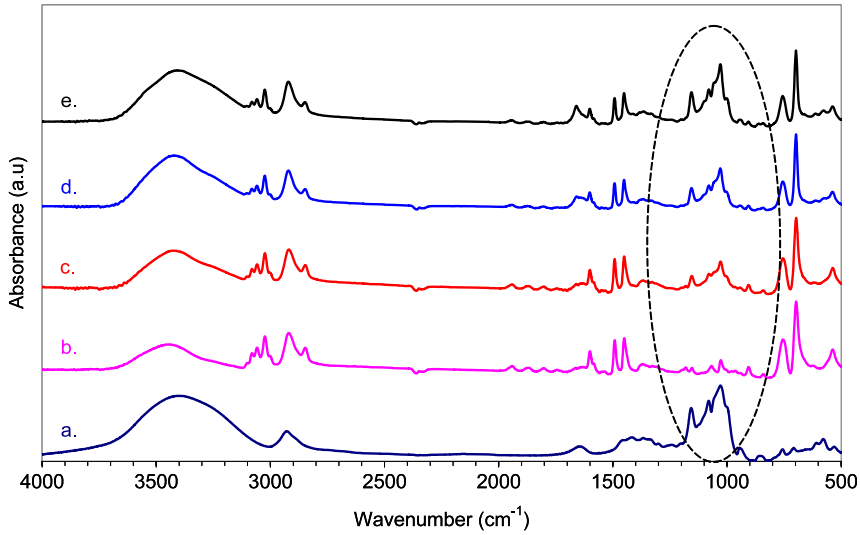


**Figure 13.** FTIR spectra of (a) pure $\beta$-CD, (b) PS25, (c) PS20/CD10, (d) PS15/CD25, and (e) PS10/CD50 fibers.

is consistent with the viscosity data as discussed previously. During electrospinning, it is also possible that CD molecules could phase separate from the PS matrix and form crystal aggregates. For instance, we tried to prepare a homogeneous film from PS/CD solutions by spin coating or solvent casting methods, but we failed since the CD molecules were phase separated and formed crystal aggregates immediately during the solvent evaporation. This is likely, since CD has a hydrophilic characteristic and PS is a hydrophobic polymer. Therefore, in the case of phase separation of CD molecules during electrospinning, it is possible that CD molecules can form crystal aggregates in the fiber matrix. However, the XRD results mainly showed broad halo diffraction features for PS/CD nanowebs containing $\beta$-CD below 50% (w/w), indicating that the CD molecules were distributed in the PS matrix without forming any crystal aggregates. This is also a good indication revealing that the cavities of CD molecules are not blocked and are supposedly available for inclusion complexation. However, some weak peaks were observed for PS/CD webs with 50% (w/w) CD, indicating that only at very high $\beta$-CD content was some amount of crystalline aggregation present.

To provide further evidence of the presence of CD molecules within the PS/CD fibers, chemical analysis was performed using Fourier transform infrared spectroscopy (FTIR). The FTIR spectra of PS and PS/CD fibers are shown in figure 13. The FTIR spectrum of pure $\beta$-CD is also shown for comparison (figure 13(a)). $\beta$-CD has characteristic absorption bands at 1028, 1080, and 1158 $cm^{-1}$, corresponding to the coupled C–C/C–O stretching vibrations and the antisymmetric stretching vibration of the C–O–C glycosidic bridge. For the PS web, the absorption bands at 2923 and 2851 $cm^{-1}$ are due to the asymmetric and symmetric stretching vibrations of $CH_2$, respectively. The prominent absorption peaks at 1452 and 1492 $cm^{-1}$ are due to the stretching vibration of the C–C bonds in the benzene ring of PS (figure 13(b)). The FTIR

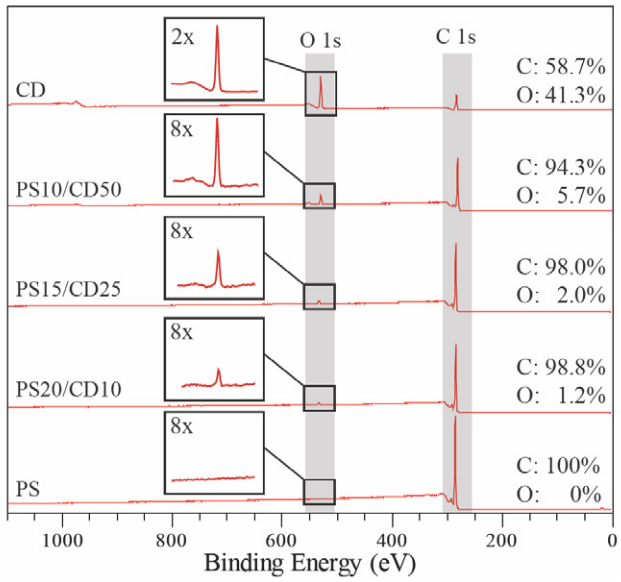


**Figure 14.** XPS wide energy survey spectra for pure PS, pure $\beta$-CD, and the three PS/CD fiber samples. The atomic concentrations of carbon and oxygen are calculated based on these spectra and shown above each spectrum to the right.

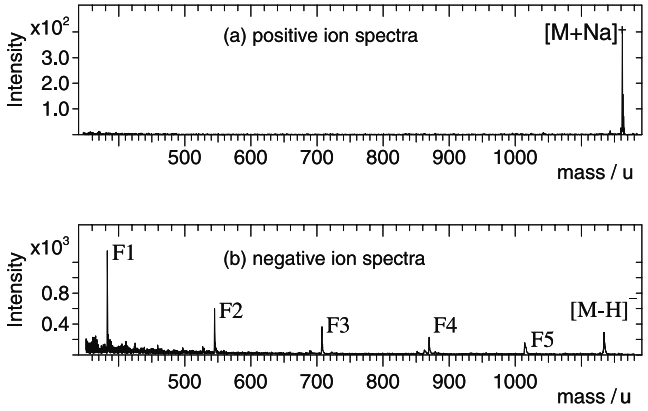


**Figure 15.** Representative positive (a) and negative (b) ion ToF-SIMS spectra in the medium mass range for a PS/CD fiber sample (PS15/CD25).

spectra of PS/CD fibers show the characteristic absorption peaks of CD, confirming that CD molecules have been successfully incorporated in PS fibers, with the peak intensity being higher for the PS/CD fibers with higher $\beta$-CD content (figures 13(c)–(e)).

Surface characterization of PS/CD nanowebs using x-ray photoelectron spectroscopy (XPS) and time-of-flight secondary ion mass spectrometry (ToF-SIMS) was performed in order to elucidate whether CD molecules were present at the fiber surface, an important property for efficient filtration. Figure 14 shows representative wide energy survey spectra for a series of different PS/CD fibers, including pure $\beta$-CD and PS fibers. Pure PS fibers do not contain oxygen (figure 14, bottom spectrum), while a high oxygen content is detected from a film of pure $\beta$-CD (figure 14, top spectrum). Thus, the appearance of an oxygen content provides evidence of the surface content of $\beta$-CD on the PS fiber surfaces. The data show a gradual increase in the surface CD content as the solution concentration increases from 10 to 50% with respect to PS; however, PS dominates the surface, and even at high CD concentrations only 5.7% of oxygen is detected. The surface CD content for all three PS/CD samples is substantially lower than the CD content of the solutions they were prepared from, indicating that most of the $\beta$-CD molecules are buried in the bulk of the fibers, so optimization of the experimental parameters for obtaining highly efficient fibers with high CD content on the fiber surfaces is desired to improve the filtration efficiency of these fibrous membranes. The improvement of CD content on the fiber surfaces may possibly be achieved by varying the spinning conditions and parameters such as the electrospinning temperature and/or using different solvent/co-solvent systems, etc. An alternative approach might be to use chemically modified CD derivatives which tend to phase segregate to the fiber surface during solvent evaporation under the applied electrospinning conditions.

In order to confirm whether the oxygen detected in the XPS studies is derived from surface $\beta$-CD molecules and to provide even more surface sensitivity (i.e. 1–2 nm for ToF-SIMS, compared to 10 nm for XPS), ToF-SIMS analysis was performed. Positive and negative ion ToF-SIMS spectra recorded from the PS15/CD25 fibers are shown in figure 15 as an example. In the positive ion spectrum, the $\beta$-CD is identified by a peak at the $m/z$ value 1157.3 corresponding to the Na adduct molecular ion of the $\beta$-CD molecule ($C_{42}H_{70}O_{35}Na^+$). In the negative ion spectrum, the dehydrogenized CD molecule is identified by a peak at the $m/z$ value 1133.7, marked $[M–H]^-$ ($C_{42}H_{69}O_{35}^-$). Peaks marked F1–F5 at $m/z$ values 383.2, 545.2, 707.3, 869.6, and 1013.8 correspond to large fragment ions of $\beta$-CD: $C_{14}H_{23}O_{12}^-$, $C_{20}H_{33}O_{27}^-$, $C_{26}H_{43}O_{22}^-$, $C_{32}H_{53}O_{27}^-$, and $C_{42}H_{62}O_{28}^-$, respectively. Similar spectra are observed for all PS/CD combinations. Thus, $\beta$-CD is present in the outer molecular layers of the PS fiber matrix and is thus available for complexation with organic molecules for filtration. This finding strongly indicates that PS/CD fibrous webs may be used as molecular filters and/or nanofilters, for example in filtration/purification/separation processes. In fact, our studies revealed that PS/CD nanowebs are very effective for capturing organic molecules (e.g. phenolphthalein) from solution [22].

## 4. Conclusions

Electrospinning of cyclodextrin functionalized PS nanofibers (PS/CD) was carried out with the goal of developing functional nanowebs. The electrospinning conditions were optimized to produce bead-free PS/CD fibers by varying the concentrations of PS (10% to 25% w/v, with respect to solvent) and $\beta$-CD (1% to 50% w/w, with respect to polymer) in the PS/CD solutions. It was observed that the presence of cyclodextrin in the PS solutions assists the electrospinning of bead-free fibers from lower polymer concentrations, and this behavior was attributed to the higher conductivity of the PS/CD solutions.

That is to say, 10% to 20% (w/v) PS solutions without $\beta$-CD yielded beaded fibers, whereas $\beta$-CD containing solutions with the same PS concentration were electrospun into bead-free uniform fibers. The morphological findings of fibers by the use of a TEM and an AFM revealed that the surface of the PS/CD fibers is rougher when compared to PS fibers. The thermal investigation of PS/CD fibers by TGA and DP-MS confirmed the presence of $\beta$-CD in the PS fibers and revealed their behaviors. XRD data suggested that $\beta$-CD molecules were mostly homogeneously distributed within the PS nanofibers without forming phase separated crystalline aggregates. Confirmation of the presence of $\beta$-CD in the bulk of the fibers was also provided by FTIR spectroscopy. Surface characterization by XPS and ToF-SIMS revealed that some $\beta$-CD molecules were located on the surface of the webs. This indicates that these CD functionalized PS webs may be utilized as molecular filters and/or nanofilters in filtration/purification/separation processes.

## Acknowledgments

We gratefully acknowledge the funding to the current project NanoNonwovens from The Danish Advanced Technology Foundation, the collaboration with Fibertex A/S, and the Danish Research Agency for the funding to the iNANO center. We also thank Yusuf Nur for help in performing the DP-MS experiments.

## References

[1] Greiner A and Wendorff J H 2007 *Angew. Chem. Int. Edn* **46** 5670–703
[2] Li D and Xia Y 2004 *Adv. Mater.* **16** 1151–70
[3] Roso M, Sundarrajan S, Pliszka D, Ramakrishna S and Modesti M 2008 *Nanotechnology* **19** 285707
[4] Bai J, Li Y X, Yang S T, Du J S, Wang S G, Zhang C Q, Yang Q B and Chen X S 2007 *Nanotechnology* **18** 305601
[5] Huang Z M, Zhang Y Z, Kotaki M and Ramakrishna S 2003 *Compos. Sci Techol.* **63** 2223–53
[6] Pham Q P, Sharma U and Mikos A G 2006 *Tissue Eng.* **12** 1197–211
[7] Barhate R S and Ramakrishna S 2007 *J. Membr. Sci.* **296** 1–8
[8] Ramakrishna S, Fujihara K, Teo W E, Yong T, Ma Z and Ramaseshan R 2006 *Mater. Today* **9** 40–50
[9] Onozuka K, Ding B, Tsuge Y, Naka T, Yamazaki M, Sugi S, Ohno S, Yoshikawa M and Shiratori S 2006 *Nanotechnology* **17** 1026–31
[10] Szejtli J 1998 *Chem. Rev.* **98** 1743–53
[11] Hedges A R 1998 *Chem. Rev.* **98** 2035–44
[12] Del Valle E M M 2004 *Process Biochem.* **39** 1033–46
[13] Harada A, Okada M, Li J and Kamachi M 1995 *Macromolecules* **28** 8406–11
[14] Uyar T, Rusa C C, Hunt M A, Aslan E, Hacaloglu J and Tonelli A E 2005 *Polymer* **46** 4762–75
[15] Wenz G, Han B-H and Muller A 2006 *Chem. Rev.* **106** 782–817
[16] Ahn Y C, Park S K, Kim G T, Hwang Y J, Lee C G, Shin H S and Lee J K 2006 *Curr. Appl. Phys.* **6** 1030–5
[17] Olah J, Cserhati T and Szejtli J 1988 *Water Res.* **22** 1345–51
[18] Crini G and Morcellet M 2002 *J. Sep. Sci.* **25** 789–813
[19] Blach P, Fourmentin S, Landy D, Cazier F and Surpateanu G 2008 *Chemosphere* **70** 374–80
[20] Kaur S, Kotaki M, Ma Z, Gopal R and Ramakrishna S 2006 *Int. J. Nanosci.* **5** 1–11
[21] Uyar T, Balan B, Toppare L and Besenbacher F 2008 *Polymer* **50** 475–80
[22] Uyar T, Havelund R, Nur Y, Hacaloglu J, Besenbacher F and Kingshott P 2008 *J. Membr. Sci.* doi:10.1016/j.memsci.2009.01.047
[23] Jarusuwannapoom T, Hongroijanawiwat W, Jitjaicham S, Wannatong L, Nithitanakul M, Pattamaprom C, Koombhongse P, Rangkupan R and Supaphol P 2005 *Eur. Polym. J.* **41** 409–21
[24] Horský J 1998 *Polym. Bull.* **41** 215–21
[25] Hunt M A, Jung D-W, Shamsheer M, Uyar T and Tonelli A E 2004 *Polymer* **45** 1345–7
[26] Uyar T, Gracz H S, Rusa M, Shin I D, El-Shafei A and Tonelli A E 2006 *Polymer* **47** 6948–55
[27] Lin T, Wang H, Wang H and Wang X 2004 *Nanotechnology* **15** 1375–81
[28] Uyar T and Besenbacher F 2008 *Polymer* **49** 5336–43
[29] Megelski S, Stephens J S, Chase D B and Rabolt J F 2002 *Macromolecules* **35** 8456–66
[30] Eda G and Shivkumar S 2007 *J. Appl. Polym. Sci.* **106** 475–87
[31] Rusa C C, Bullions T A, Fox J, Porbeni F E, Wang X and Tonelli A E 2002 *Langmuir* **18** 10016–23
[32] Uyar T, Aslan E, Tonelli A E and Hacaloglu J 2006 *Polym. Degrad. Stab.* **91** 1–11
[33] Uyar T, Rusa C C, Tonelli A E and Hacaloglu J 2007 *Polym. Degrad. Stab.* **92** 32–43
[34] Baker S C, Atkin N, Gunning P A, Granville N, Wilson K, Wilson D and Southgate J 2006 *Biomaterials* **27** 3136–46
[35] Saenger W, Jacob J, Gessler K, Steiner T, Hoffmann D, Sanbe H, Koizumi K, Smith S M and Takaha T 1998 *Chem. Rev.* **98** 1787–802
[36] Harata K 1998 *Chem. Rev.* **98** 1803–27